CHEMISTRY OF MATERIALS

pubs.acs.org/cm

Article

Mechanistic Study on Thermally Induced Lattice Stiffening of ZIF-8

Jian Hao, Deepu J. Babu, Qi Liu, Pascal Alexander Schouwink, Mehrdad Asgari, Wendy L. Queen, and Kumar Varoon Agrawal*

Cite This: *Chem. Mater.* 2021, 33, 4035−4044

Read Online

ACCESS | Metrics & More | Article Recommendations | Supporting Information

ABSTRACT: The flexibility of the ZIF-8 aperture, which inhibits a molecular cutoff of 3.4 Å, can be reduced by rapid heat treatment to obtain CO_2-selective membranes. However, the early stages of the structural, morphological, and chemical changes responsible for the lattice rigidification remain elusive. Herein, using *ex situ* and *in situ* experiments, we determine that a small shrinkage of the unit-cell parameter, ∼0.2%, is mainly responsible for this transformation. Systematic gas permeation studies show that one needs to achieve this shrinkage without a disproportionately large shrinkage in the grain size of the polycrystalline film to avoid the formation of cracks. We show that this condition is uniquely achieved in a short time by exposure of ZIF-8 to a mildly humid environment where lattice parameter shrinkage is accelerated by the incorporation of linker vacancy defects, while the shrinkage in grain size is limited. The water-vapor-led incorporation of linker vacancy defects takes place with an energy barrier of 123 kJ mol^{-1}, much higher than that for the thermal degradation of ZIF-8, <80 kJ mol^{-1}. The latter is promoted by heat treatment in a dry environment at a relatively higher temperature; however, this condition does not shrink the lattice parameters at short exposure time.

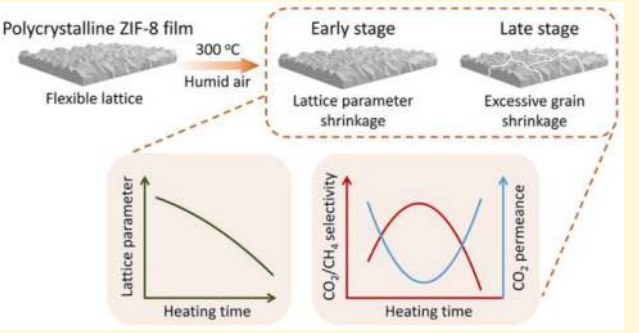

1. INTRODUCTION

Zeolitic imidazolate framework-8 (ZIF-8), which hosts 3.4-Å-sized windows composed of six-membered rings of Zn nodes coordinated to 2-methylimidazole (Hmim), is a highly promising metal−organic framework (MOF) for a number of molecular separations.[1−8] To improve the separation performance, several synthetic approaches focusing on the optimization of the host−guest interaction, for example, molecular diffusivity, have been reported.[8−12] In the case of polycrystalline ZIF-8 membranes, optimized separation performance has been achieved by inducing lattice distortion[13−16] and linker[9,12] and metal heterogeneities[17] as well as by engineering morphology (grain size,[18] orientation,[19] film thickness,[20] etc.[21−23]). Unfortunately, almost all of these studies were negatively impacted by the framework flexibility of ZIF-8,[24,25] which allows the diffusion of molecules much larger than its 3.4 Å window, e.g., N_2, CH_4, C_3H_6, C_3H_8, *n*-C_4H_{10}, and so on. As a result, despite the considerable difference in size between CO_2 (3.3 Å), N_2 (3.64 Å), and CH_4 (3.8 Å), CO_2/N_2 and CO_2/CH_4 selectivities of polycrystalline ZIF-8 membranes have been limited,[26] although postsynthetic linker exchange based approaches have improved molecular-sieving performance.[12]

To overcome the aforementioned issue, we recently developed a postsynthetic strategy, rapid heat treatment (RHT), which stiffens the ZIF-8 lattice leading to significantly improved selectivities of the gas pairs CO_2/N_2 and CO_2/CH_4 by simply heating the as-synthesized membrane at around 360 °C for a few seconds.[27] The transformation was characterized by a large increase in the activation energy for gas transport. In fact, larger molecules such as C_3H_6 and C_3H_8 were completely blocked.

It is important to note that the lattice transformation upon a short-term heat treatment at a moderate temperature (300−360 °C) in the case of RHT is quite distinct from the treatment at higher temperatures (>400 °C) where a significant thermal degradation of ZIF-8 takes place. For example, Koros and co-workers reported a 2−3 orders of magnitude increase in the diffusivities of SF_6, *n*-butane, and isobutane when ZIF-8 was treated at 400−500 °C in argon for 2 h.[28] Gadipelli et al.[29] found that ZIF-8 shows improved CO_2 uptake and CO_2/N_2 adsorption selectivity after heating at the temperature as high as 525 °C under argon for 3 h. On the basis of the X-ray diffraction (XRD) data, they reported that the crystalline structure of ZIF-8 was maintained at 525 °C; however, there was a slight peak shift/broadening observed in the diffraction pattern. Also, an amorphous material was obtained at 550 °C. Moreover, Lin and co-workers established that ZIF-8 crystallinity decreases at temperatures above 200 °C in several environments[30−32] when it is annealed for 20 h. Importantly, these experiment were

Received: February 8, 2021
Revised: March 29, 2021
Published: May 19, 2021

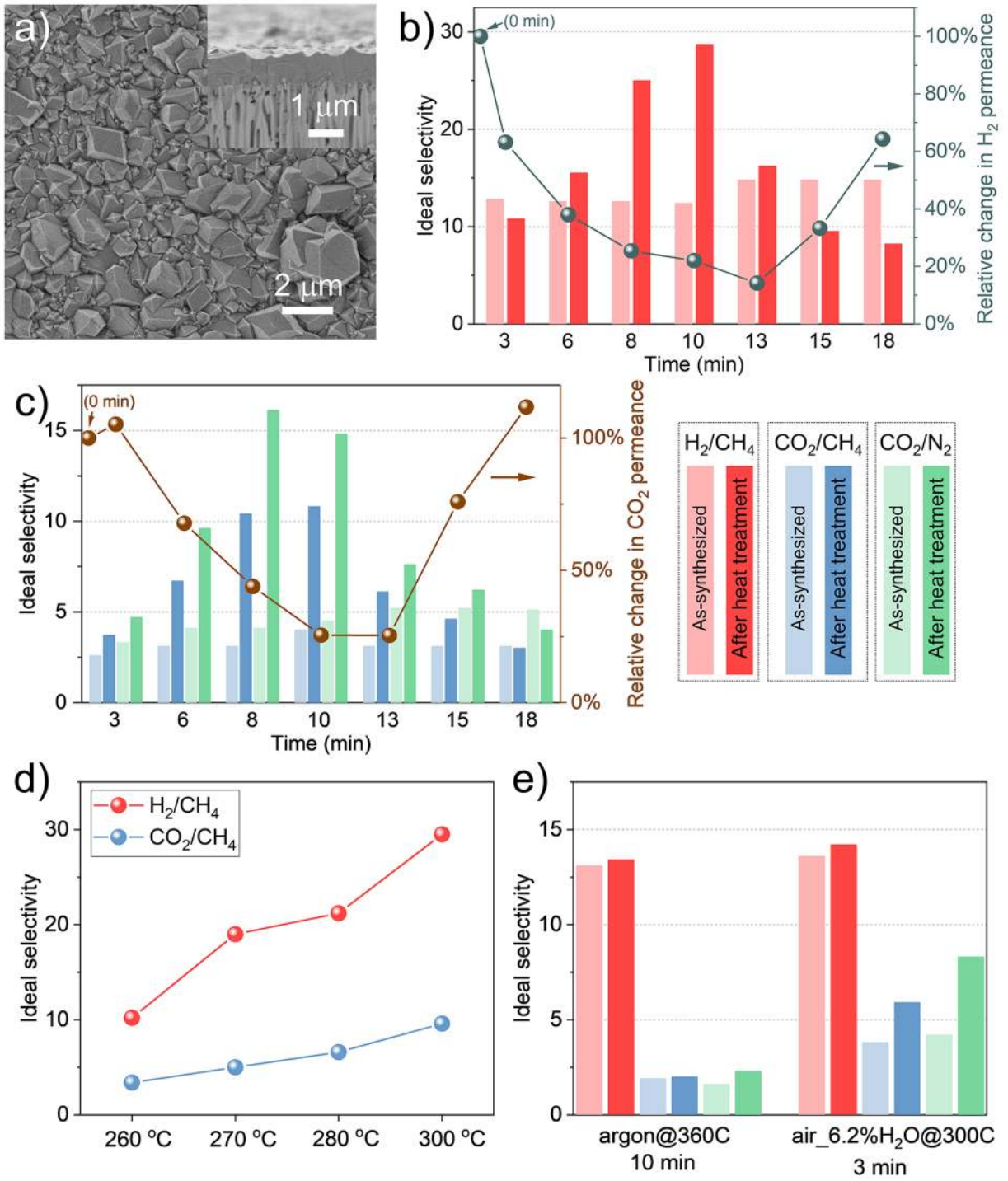

Figure 1. (a) SEM image of the ZIF-8 membrane synthesized in this work. The inset is the cross-sectional view of the membrane. (b) H_2/CH_4 and (c) CO_2/CH_4 and CO_2/N_2 ideal selectivities and the corresponding change in the H_2 (b) and CO_2 (c) permeances from polycrystalline ZIF-8 membranes after heat treatment in air_1.0%H_2O@300C for dwell times of 3−18 min. (d) H_2/CH_4 and CO_2/CH_4 ideal selectivities from heat-treated ZIF-8 membranes as a function of temperature in air_1.0%H_2O for a treatment time of 10 min. (e) Change in the ideal selectivity after heat treatment in argon@360C for 10 min and air_6.2%H_2O@300C for 3 min. All of the permeation data were collected at 25 °C and 1.4 bar.

performed under isothermal conditions in contrast to the conventional dynamic temperature ramping approach commonly used in the thermogravimetric analysis.

Overall, most studies on the thermal treatment of ZIF-8 have focused on its structural degradation at relatively high temperatures (>400 °C)[33−36] and/or at a relatively long soaking time (>20 h).[28−32,37] As we show later, these conditions are too harsh for polycrystalline membranes and lead to a severe crack formation. As an exception, Pan et al. discussed size shrinkage of ZIF-8 at 300 °C in air for 2 h; however, the dry conditions are not effective in inducing lattice stiffening (as we demonstrate in this study).[38] Given this, a systematic study focused on the early stages of the ZIF-8 transformation (lattice parameters, grain/crystal size, chemical composition, defect formation, etc.) is needed to understand the origin of lattice stiffening and resulting enhancements in the molecular selectivity.

https://doi.org/10.1021/acs.chemmater.1c00455
Chem. Mater. 2021, 33, 4035−4044

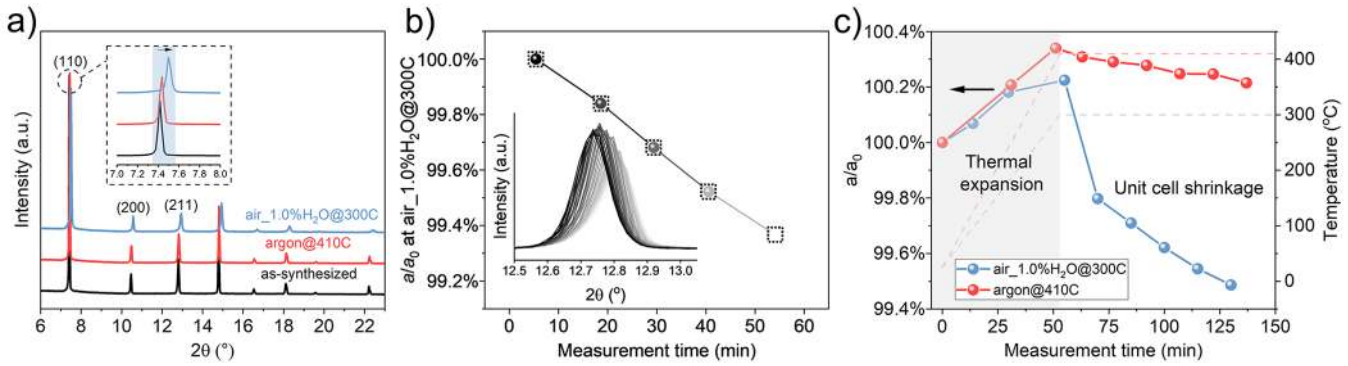

Figure 2. (a) *Ex situ* XRD patterns of the as-synthesized ZIF-8 crystals and those after heating in air_1.0%H_2O@300C and argon@410C for 2 h. The ratio change of the *a*-axis obtained from *in situ* XRD measurement of ZIF-8 crystals after (b) directly heating in air_1.0%H_2O@300C and (c) heating from room temperature to air_1.0%H_2O@300C and argon@410C. The inset in (b) is the XRD patterns of the ZIF-8 (211) peak.

In this work, we study the effect of temperature and atmosphere (dry, humid, nonoxidizing) on the structural (lattice parameters, microporosity), compositional (linker vacancy defects, transformation to ZnO), and morphological changes (grain-boundary defects, crack formation, size shrinkage of single crystals) of ZIF-8. We find that lattice stiffening is only manifested in increased gas pair selectivity when the polycrystalline ZIF-8 membrane is treated under a slightly humid environment (1.0% water vapor). Also, there is an optimal duration of the heat treatment process; the selectivity first increases with the heating time due to lattice stiffening and then begins to drop due to the formation of grain-boundary defects and nanoscale cracks resulting from a shrinkage of the grain size. We show that lattice stiffening is mainly driven by a significant reduction in unit-cell parameters, which in turn coincides with the incorporation of linker-vacancy defects and size shrinkage of the crystals. In the absence of humidity, unit-cell parameter changes are minimal and linker-vacancy defects are absent.

2. RESULTS AND DISCUSSION

Polycrystalline ZIF-8 films anchored to a porous support were synthesized by the electrophoretic nuclei assembly for crystallization of highly intergrown thin films (ENACT) approach (Figure 1a).[22,23] As-synthesized membranes yielded H_2 and CO_2 permeances of 2×10^{-6} and 5×10^{-7} mol m^{-2} s^{-1} Pa^{-1}, respectively, and H_2/CH_4, CO_2/CH_4, and CO_2/N_2 ideal gas selectivities of 13.2, 3.2, and 4.0, respectively (Tables S1.1−S1.3), values that are typical of high-quality polycrystalline ZIF-8 membranes.[39] The gas transport property of these membranes was systematically investigated as a function of heat treatment where parameters including heating atmosphere, temperature, and dwell time were varied.

When the membranes were exposed to 300 °C in air with a water vapor content of 1.0% (the condition and temperature hereafter termed "condition"@*T*, i.e., air_1.0%H_2O@300C in this case) at different dwell times, a noteworthy trend in the transport behavior was observed (Figure 1b,c and Table S1.1). At first, for a short treatment time (dwell time of 3−13 min), there was a monotonic increase in selectivities; H_2/CH_4 increased from 13.2 to 28.7, CO_2/N_2 increased from 3.2 to 10.8, and CO_2/CH_4 increased from 4.0 to 16.1. This was accompanied by a monotonic decrease in the H_2 and CO_2 permeances; this behavior indicates a progressive lattice stiffening with dwell time. Next, the reverse trend of decreasing selectivity and increasing permeance is observed when the dwell time is further increased. Scanning electron microscopy (SEM) images of the sample at a long dwell time (18 min, Figure S2a) revealed significant grain-boundary defects which subsequently transform into cracks upon extended exposure to the electron beam (Figure S2b). We observed a few cracks propagating a section of the membrane when the dwell time was higher (20 min, Figure S3a). Interestingly, when these cracks were covered by a defect sealing layer of poly[1-(trimethylsilyl)-1-propyne] or PTMSP (footnotes in Table S1.1), the film yielded a high H_2/CH_4 selectivity of 34.9 (membrane M8 in Table S1.1), indicating that grain-boundary defects and cracks are primarily responsible for deteriorating the selectivity at the longer dwell time. When the cracks were severe, for example, in the case of a 30 min dwell time (Figure S3b), the defect sealing was not effective, and the resulting H_2/CH_4 and CO_2/CH_4 selectivities (3.1 and 3.0) reflected that expected from a stand-alone PTMSP film.[40]

The effect of heat treatment on the performance of ZIF-8 membranes was further examined as a function of temperature while keeping the dwell time as 10 min. Figure 1d shows that H_2/CH_4 and CO_2/CH_4 selectivities monotonically increased with the temperature in the range 260−300 °C. At the lowest temperature (260 °C), the membrane performance barely changes from that of the as-synthesized membrane (membrane M9 in Table S1.2), while at a slightly higher temperature (300 °C), H_2/CH_4 and CO_2/CH_4 selectivities of 30 and 10, respectively, were obtained (membranes M4 and M12 in Tables S1.1 and 1.2). Increasing the temperature to 330 °C resulted in a severely cracked film, indicating that the rate of chemical and structural changes taking place in ZIF-8 accelerated at higher temperature (Figure S4).

The importance of humidity on the membrane performance was investigated by treating the ZIF-8 membranes in dry and higher humidity environments (dry argon and air_6.2%H_2O, in contrast to air_1.0%H_2O). Interestingly, heat treatment in argon@360C for 10 min led to neither an improvement in the separation performance (Figure 1e, M13 in Table S1.3) nor crack development (Figure S5), in striking contrast to observations in air_1.0%H_2O. This indicates that the severe crack formation in air_1.0%H_2O@330C (Figure S4) is not caused by the mismatch in the thermal expansion coefficient between the porous support and the polycrystalline ZIF-8 film but rather originates from the structural and chemical changes in ZIF-8 upon exposure to air_1.0%H_2O. It also emphasizes the important role humidity has in optimizing membrane performance.

https://doi.org/10.1021/acs.chemmater.1c00455
Chem. Mater. 2021, 33, 4035−4044

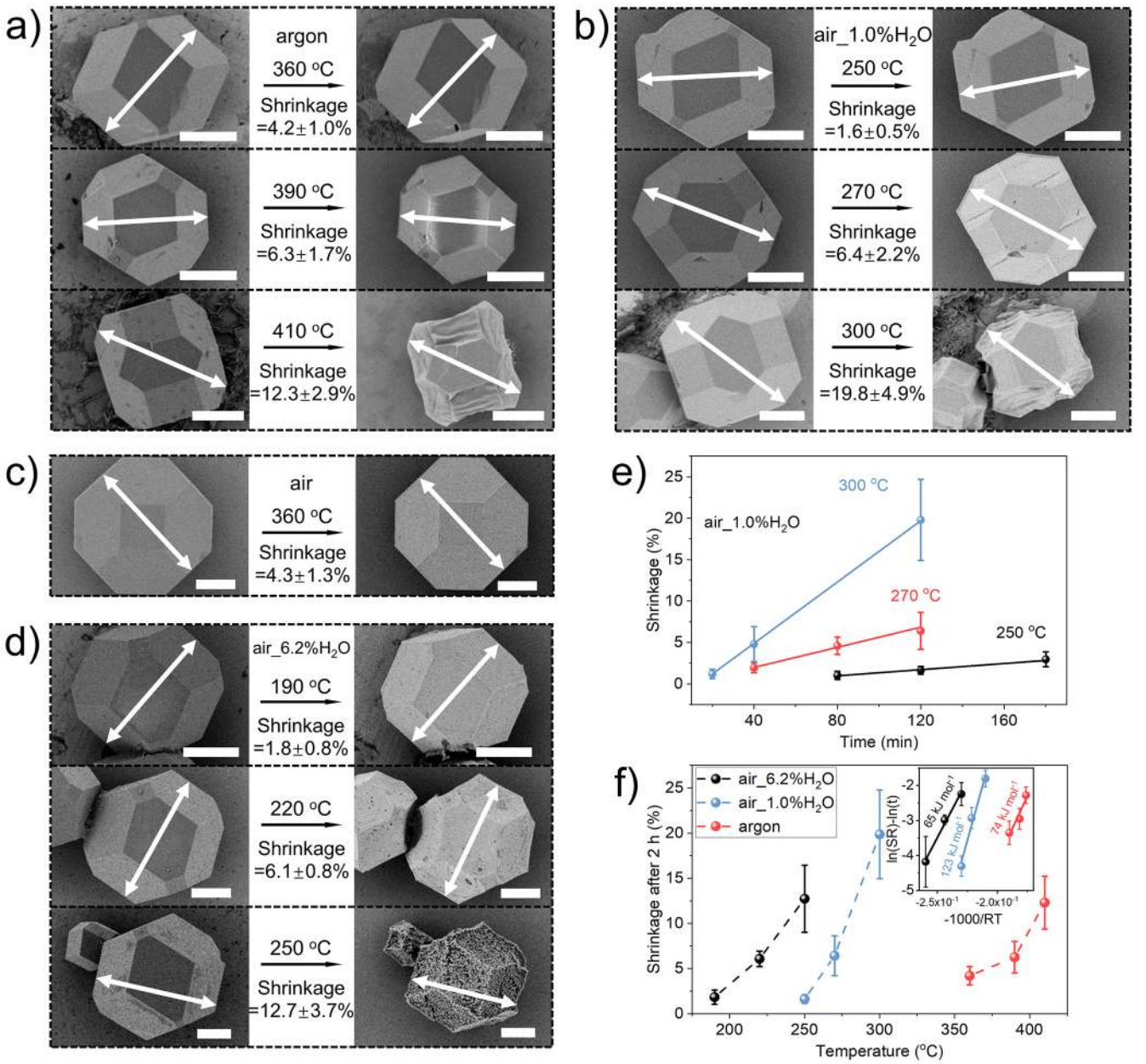

Figure 3. SEM images of ZIF-8 crystals before and after heat treatment in (a) argon for 2 h at 360, 390, and 410 °C; (b) air_1.0%H_2O for 2 h at 250, 270, and 300 °C; (c) dry air for 2 h at 360 °C, and (d) air_6.2%H_2O for 2 h at 190, 220, and 250 °C. The shrinkage was calculated based on the size change on the same crystal. All scale bars: 5 μm. Summarized shrinkage of ZIF-8 crystals (e) treated in air_1.0%H_2O for different durations at 250, 270, and 300 °C and (f) treated for 2 h under different atmospheres. The inset is the calculated activation energy based on the shrinkage according to the Arrhenius equation. The solid lines represent the linear fitting results.

At higher humidity (air_6.2%H_2O@300C), a noticeable increase in selectivities was observed, in a very short time (3 min), with CO_2/CH_4 and CO_2/N_2 selectivities increasing from 3.8 to 5.9 and 4.2 to 8.3, respectively (membrane M14 in Table S1.3). Upon increasing the dwell time to 10 min, the membranes developed a large number of cracks (Figure S7), similar to when the membrane was exposed to air_1.0%H_2O@300C at much longer dwell times (>30 min). This indicates that increasing humidity accelerates the structural changes in ZIF-8.

A shrinkage in the lattice parameter upon heat treatment under humid environment could explain the above-observed lattice stiffening behavior. Therefore, we performed powder diffraction experiments on heat-treated ZIF-8. The XRD pattern of as-synthesized ZIF-8 matched well with that in the literature (Figure 2a).[1] Upon exposure to air_1.0%H_2O@300C for 2 h, all peaks shifted to a higher 2θ position (Figure 2a and Figure S8) corresponding to 1.1% shrinkage in the lattice parameter (Table S2). The relative changes in the lattice parameter derived from (110), (200), and (211) planes are consistent, indicating that the shrinkage of the ZIF-8 lattice was isotropic. In the case of the dry argon environment, we could only observe minor shrinkage (0.2%, Table S2) after heating for 2 h but using a much higher temperature (410 °C, Figure 2a and Figure S8). Assuming that lattice stiffening is correlated to the relative unit cell shrinkage, this observation is consistent with the gas selectivity data (Figure 1e).

The lattice shrinkage was further verified by *in situ* XRD experiments. In the first *in situ* experiment, ZIF-8 powder was

https://doi.org/10.1021/acs.chemmater.1c00455
Chem. Mater. 2021, 33, 4035−4044

heated to 300 °C in argon, following which the environment was changed to air_1.0%H_2O while maintaining the temperature. The resulting shifts in the (211) peak and shrinkage of the *a*-axis are plotted as a function of exposure time to air_1.0%H_2O in Figure 2b. These shifts were a monotonic function of the dwell time in humid air (5−55 min). For a short dwell time of 20 min, which is relevant to the membrane experiments, the peak shifted from 2θ of 12.732 to 12.755 corresponding to a shrinkage of 0.2% of the *a*-axis parameter, indicating that minor lattice shrinkage is enough to induce lattice stiffening. For the longest dwell time of 55 min, the corresponding shrinkage in the lattice parameter was 0.7%. Interestingly, when the experiment was repeated under the dry air conditions, the lattice parameter shrinkage was much less; it took 55 min to observe a shrinkage of 0.3% (Figure S9). This highlights that humidity places an important role in achieving the needed shrinkage in the short period of time.

In the second *in situ* experiment, ZIF-8 was heated in a fixed environment from room temperature to a set temperature (300 °C for air_1.0%H_2O and 410 °C for dry argon) in 50 min, after which the sample was held isothermally at the set temperature. During the first 50 min of the measurement where temperature ramped to the set temperature, the a/a_0 ratio increased attributing to the positive thermal expansion coefficient of ZIF-8 (Figure 2c and Figure S10).[41] During the isothermal stage of the experiment, the lattice parameter shrank for both humid and dry environments. Consistent with *ex situ* experiments, the decrease in the lattice parameter was much larger in humid environment compared to that in the dry environment, reaching ∼0.4% in 25 min and ∼0.7% in 70 min compared to only 0.1% after 70 min in dry argon.

The lattice flexibility of ZIF-8 is known to arise from the flip-flop vibrational mode of 2-methylimidazole (also known as gate-opening phenomena),[24] and the observed reduction in the lattice parameter, with the aid of the *ex situ* and *in situ* XRD experiments, is expected to restrict this vibration.[27] These aforementioned experiments confirm that heating samples for short periods of time in the presence of humidity is important to realize the shrinkage in the lattice parameters in a rapid way, which is required to reduce the lattice flexibility while avoiding the crack formation in the polycrystalline ZIF-8 films.

Next, to gain the understanding of the underlying changes in ZIF-8, which in turn generates grain boundary defects and eventually cracks in the membranes at a longer dwell time, we performed a systematic study of the size changes in various heating environments. To this end, well-faceted 5−25 μm sized ZIF-8 crystals were synthesized by using the formate-modulated solvothermal approach.[39,42,43] The crystals had the typical truncated rhombic dodecahedron shape with six symmetry-equivalent (100) and twelve (110) facets (Figure S11).[42,44] The size of the crystal was measured by the distance between the two opposite (110) facets. Only crystals with a clear top view in the SEM image were selected for the size analysis, and the analysis was performed on the same set of crystals before and after the heat treatment.

Upon treatment in argon@360C for 2 h, the ZIF-8 crystal underwent a shrinkage of 4.2 ± 1.0% (Figure 3a). At identical dwell time, this shrinkage increased upon increasing the temperature, i.e., 6.3 ± 1.7% at 390 °C and 12.3 ± 2.9% at 410 °C. The presence of humidity in the environment (air_1.0% H_2O) resulted in crystals shrinking more aggressively, and the size reduction could be observed at much lower temperatures. The shrinkage was 1.6 ± 0.5% (250 °C), 6.4 ± 2.2% (270 °C), and 19.8 ± 4.9% (300 °C) for the same dwell time. The shrinkage was isotropic; i.e., the distance between the opposite (100) facets was similar to that of opposite (110) facets (Figure S12). However, when the shrinkage was higher than 7%, the crystal shape distorted (Figure 3a,b), likely due to structural collapse. When the amount of water vapor was increased to 6.2% in air (Figure 3d), the size shrinkage could be observed at even lower temperatures; i.e., 1.8 ± 0.8%, 6.1 ± 0.8%, and 12.7 ± 3.7% of shrinkage were observed at 190, 220, and 250 °C, respectively. The trend of the size shrinkage is in good agreement with that of the weight loss of ZIF-8 as shown in Figure S13.

To understand whether the aggressive shrinkage in air_1.0% H_2O was mainly driven by the water vapor or air, control experiments were performed by heating in dry air for 2 h (Figure 3c). In this case, a limited shrinkage of 4.3 ± 1.3% was observed at 360 °C comparable to that observed in dry argon, ∼4%. It is noted that a recent report indicates a much larger shrinkage (29%) of ZIF-8 after exposure to a dry environment at 300 °C for 2 h.[38] Our results imply that their observation was largely influenced by the damage induced by the high-energy beam of the transmission electron microscope that was used for imaging and calculating shrinkage.

Plotting shrinkage as a function of time revealed a linear progression (Figure 3e). For example, the shrinkage increased linearly as a function of time at 250, 270, and 300 °C in air_1.0% H_2O (Figure 3e and Figure S14) and at 410 °C in argon (Figures S15 and S16). This indicates that the ZIF-8 shrinkage kinetics are pseudo-zero-order, at least in these conditions (shrinkage ≤20%) prior to significant framework collapse. We could fit an Arrhenius-type relationship (eq 1) between the size shrinkage and the temperature when the dwell time was set to 2 h (Note S2, Figure 3f, Tables S3 and S4)

$$\frac{\mathrm{d}}{\mathrm{d}t}(\text{shrinkage}) \propto \exp\left(-\frac{E_a}{RT}\right) \tag{1}$$

where E_a is the corresponding activation energy, T is the temperature, and R is the universal gas constant. The fitted activation energy in the case of air_1.0%H_2O is 123 ± 18 kJ mol^{-1}, much higher than that reported for the thermal decomposition of ZIF-8 (73−86 kJ mol^{-1}) in several atmospheres (air, argon, H_2/CO_2, and N_2).[30] For example, E_a in air and argon environments was reported to be 86 and 74 kJ mol^{-1}, respectively. This suggests that the shrinkage of ZIF-8 in the presence of 1.0%H_2O is distinct from the thermal decomposition of ZIF-8. It is reported that in aqueous solution water can induce hydrolysis of ZIF-8 to form Zn^{2+} ions.[32] Using density functional theory calculations, Schmidt and co-workers[45] predicted that water vapor can react with ZIF-8 to form linker vacancy defects with an activation energy of 121 kJ mol^{-1}, close to the activation energy measured by this study. The above-calculated kinetics suggest that water molecules in the air likely form linker vacancy defects (verified later by using diffuse reflectance infrared Fourier transform spectroscopy and nitrogen adsorption experiment), which eventually leads to the observed shrinkage. Compared to air_1.0%H_2O, when ZIF-8 is treated in dry argon, E_a is calculated to be 74 ± 22 kJ mol^{-1}, which is in good agreement with the activation energy of thermal degradation reported by Lin and co-workers.[30]

Interestingly, when the water vapor content in air is increased to 6.2%, E_a drops to 65 ± 7 kJ mol^{-1}. This likely has an origin in ZIF-8 hydrolysis in the excess amount of water vapor. ZIF-8 has been shown to completely transform into ZnO after hydro-

https://doi.org/10.1021/acs.chemmater.1c00455
Chem. Mater. 2021, 33, 4035−4044

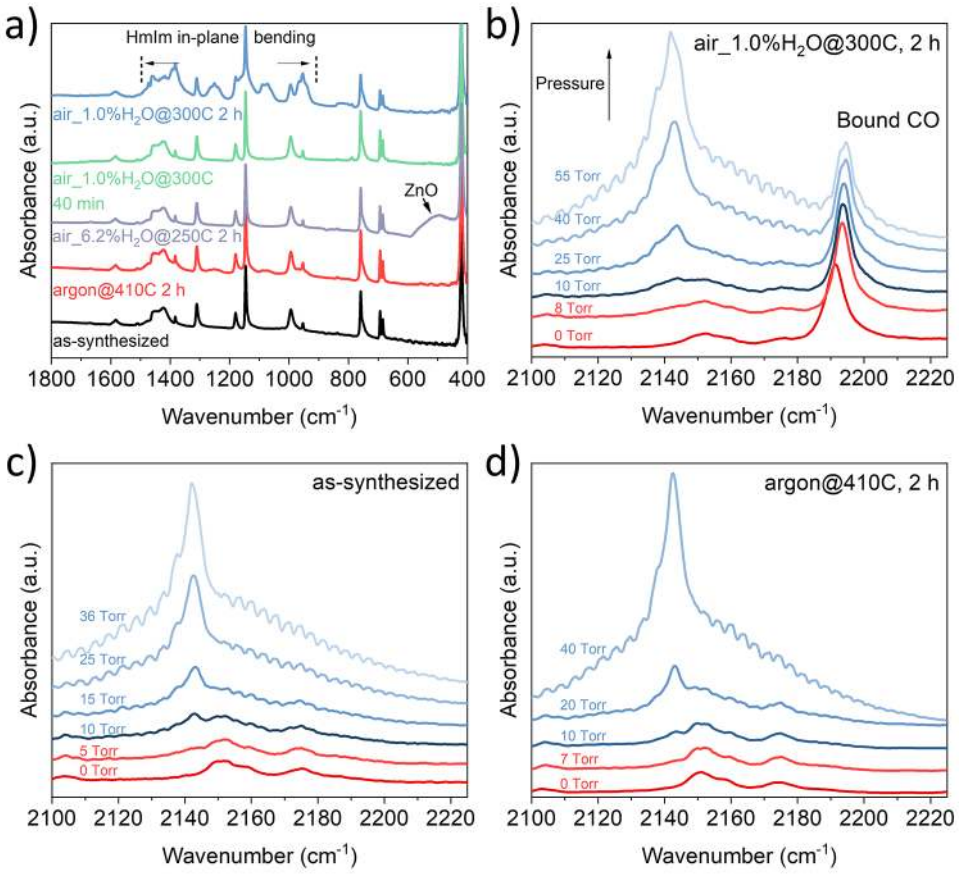

Figure 4. (a) FTIR spectra of the as-synthesized ZIF-8 and those after heating in argon@410C for 2 h, air_1.0%H_2O@300C for 40 min and 2 h, and air_6.2%H_2O@300C for 2 h. (b–d) *In situ* DRIFTS spectra obtained after by dosing ZIF-8 to CO. (b) ZIF-8 treated in air_1.0%H_2O@300C for 2 h, (c) as-synthesized ZIF-8, and (d) ZIF-8 treated in argon@410C for 2 h.

thermal treatment in water at 80 °C for 24 h.[46] Not surprisingly, XRD patterns of the ZIF-8 powder after heating in air_6.2% H_2O@250C for 2 h clearly reveal the presence of the ZnO (Figure S17). The hydrolysis is also observed by SEM (Figure 3d) where visible pores develop in ZIF-8 even at extremely low temperature, 190 °C, at a shrinkage of only 1.9%.

These observations can be summarized as follows: when heating is performed in dry environments (oxidative or nonoxidative), a detectable size reduction is only observed above 360 °C and is mainly driven by thermal decomposition. In the presence of water vapor (1.0%), the shrinkage of ZIF-8 is accelerated by the formation of linker vacancy defects, while an excess amount of water vapor (6.2%) promotes the hydrolysis of ZIF-8 to ZnO.

On the basis of this, we can explain why exposure to a mildly humid environment (1.0% water vapor) is essential to reduce the flexibility of the polycrystalline ZIF-8 film. To shrink the lattice by 0.2% required to reduce the lattice flexibility, one merely needs to heat the polycrystalline film for less than 10 min at 300 °C under mildly humid conditions, during which the grain size will barely shrink (for 5–25 μm sized ZIF-8 crystals, extrapolated from Figure 3e). Therefore, one achieves lattice shrinkage while avoiding significant grain boundary defects and cracks. On the other hand, to obtain the same shrinkage in dry conditions, one needs to heat ZIF-8 to much higher temperature (e.g., 410 °C in argon) for several hours. However, this would lead to a significant shrinkage in grain size and would generate severe cracks in the polycrystalline film.

To understand the chemical changes in ZIF-8 upon heat treatment, we characterized the heat-treated samples by the Fourier-transform infrared spectroscopy (FTIR). Data from as-synthesized ZIF-8 was compared to that from the samples treated in air_6.2%H_2O@250C and argon@410C for 2 h (12% shrinkage in these samples) and was contrasted to data from samples treated in air_1.0%H_2O@300C for 40 min and 2 h where 5 and 20% shrinkage were observed, respectively. We make the following observations (Note S3):

(i) There were no detectable chemical changes in the case of argon@410C (Figure 4a and Figure S18) despite ~12% size shrinkage. This corroborates well to minimal (0.2%) change in the lattice parameter of ZIF-8.

(ii) For samples treated in air_1.0%H_2O@300C, we observed a slight blue-shift (1 cm^{-1}) for the Zn–N coordination bond (Figure S18), indicating a stiffening of the Zn–N bond.[27] The peak corresponding to the out-of-plane bending of the ring (650–800 cm^{-1}) retained its shape; however, the peak intensity decreased for the sample treated for 2 h. This could have origin in restricted flip-flop motion of the linker. The in-plane bending (900–1300 cm^{-1}) and the ring stretching convoluted bands (1350–1500 cm^{-1})[30,47,48] changed significantly, indicating the decomposition of the HmIm ring.[30]

(iii) In the case of air_6.2%H_2O@250C, the presence of ZnO is evident, in agreement with the XRD data. Interestingly, the in-plane bending and ring stretching bands did not

https://doi.org/10.1021/acs.chemmater.1c00455
Chem. Mater. 2021, 33, 4035–4044

change indicating that the decomposition does not take place at exposure to 250 °C for 2 h.

The FTIR spectra give insights into the changes in the chemical structure of ZIF-8 upon heating. To further probe the formation of linker vacancies, we performed *in situ* diffuse reflectance infrared Fourier transform spectroscopy (DRIFTS) experiments on the as-synthesized ZIF-8 as well as ZIF-8 treated in air_1.0%H_2O@300C and argon@410C for 2 h, respectively (Figure 4b–d). To probe for the presence of open metal sites, the DRIFTS spectrum was collected for each ZIF-8 sample. Briefly, CO was dosed into the sample chamber, and measurements were taken with increasing CO pressure. It is noted that the stretching frequency for unbound CO is 2143 cm^{-1}, and when CO binds to a metal, the stretching frequency will undergo a significant blue-shift or a red-shift, which is dictated by the nature of the bonding interaction. When CO binds to an open metal, the peak is normally sharp and without periodic fluctuations upon increasing the CO pressure, in contrast to CO that is weakly bound to a solid surface (between 2130 and 2140 cm^{-1}).[49] As shown in Figure 4b, for the air_1.0% H_2O@300C sample, the stretching frequency of the bound CO appears at ~2187 cm^{-1}, which is significantly blue-shifted with respect to the stretching frequency of free CO. This indicates a nonclassical CO adsorption, which is not surprising as Zn^{2+} has a fully occupied set of 3d orbitals eliminating the metals ability to accept σ-donation from the CO molecule. This significant blue-shift is consistent with those observed in other MOFs having open Zn^{2+} coordination sites.[50] With an increase in the pressure of CO (>10 Torr), a second peak appears at ~2143 cm^{-1} as expected for free and/or weakly bound CO (Figure 4b). On the contrary, both the DRIFTS spectra of the as-synthesized ZIF-8 before (Figure 4c) and after heating in argon@410C (Figure 4d) reveal a single C–O stretch at ~2143 cm^{-1}, representative of free and/or weakly bound CO. This indicates that heating ZIF-8 in dry atmospheres even at 410 °C for 2 h does not lead to significant linker vacancies, which likely limits the shrinkage of the lattice parameters (<0.2%). However, when the sample is heated in the presence of only 1.0% water vapor even at a lower temperature (300 °C), it promotes the formation of linker vacancies, increasing the shrinkage of the lattice parameter (1.1%), and crystal size (~20%).

Finally, we investigated the nitrogen adsorption properties and specific surface area (SSA) of the as-synthesized and thermally treated ZIF-8 to gain further insight into any changes brought upon by the humid environment. The N_2 uptake data for as-synthesized ZIF-8 and those obtained after heating in air_1.0%H_2O@300C for 40 min and 2 h and in argon@410C for 2 h are shown in Figure 5a. The data reveals standard type I isotherms at low pressures indicative of a microporous structure. However, for the humid environments (40 min as well as 2 h samples), there is a deviation in the second step (P/P_0 between 3×10^{-3} and 3×10^{-2}), which is attributed to the lattice flexibility or gate-opening phenomena of ZIF-8.[24] Upon treatment in a humid environment, the second step starts to move toward higher pressures, indicating that the gate opening is becoming more difficult. This is consistent with the stiffening of coordination bonds from the reduction in the lattice parameter (0.5% and 1.1% for 40 min and 2 h samples). However, the sample treated in dry argon has a similar second step as that of the as-synthesized ZIF-8, confirming that the flexibility of ZIF-8 is not affected in the absence of humidity. The Brunauer–Emmett–Teller (BET) SSA calculated for the as-synthesized

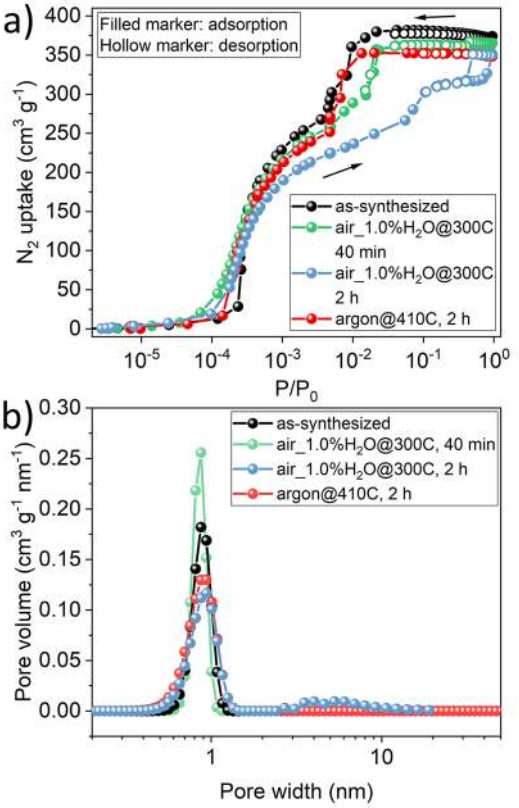

Figure 5. (a) Nitrogen adsorption/desorption isotherms of the as-synthesized ZIF-8 and those after heating in air_1.0%H_2O@300C for 40 min and 2 h and in argon@410C for 2 h, respectively, and (b) the corresponding pore size distribution calculated by the BJH method.

ZIF-8 and that treated in argon is ~1450 m^2 g^{-1} (Table S5), similar to the reported values,[1,42] while the SSA after heating in air_1.0%H_2O decreases to ~1200 m^2 g^{-1}. A similar decrease was also observed in the pore volume (from 0.578 to 0.542 cm^3 g^{-1}, Table S5). The desorption isotherm curves overlap well for the as-synthesized ZIF-8 and ZIF-8 after heating at argon@410C for 2 h and air_1.0%H_2O@300C for 40 min, while a hysteresis loop appears after heating at air_1.0%H_2O@300C for 2 h, suggesting that mesoporous structures are developing in the framework of ZIF-8. This is further evidenced by the pore-size-distribution calculated by the BJH method (Figure 5b); all of the ZIF-8 samples exhibit a pore diameter of (~1 nm), while the development of mesopores (3–10 nm) starts to become obvious only for the ZIF-8 sample after heating at air_1.0% H_2O@300C for 2 h.

3. CONCLUSION

In this work, we systematically investigated the structural, morphological, and chemical changes in ZIF-8 upon short heat treatment, highly relevant for improving the carbon capture performance of ZIF-8 membranes by stiffening the ZIF-8 lattice. We showed that a small shrinkage in the lattice parameter (0.2%), caused by humidity-driven linker vacancy defects, is the main driving force for reducing the lattice flexibility of ZIF-8. It is important to design the experiment to attain this shrinkage without generating significant grain boundary defects or cracks in the polycrystalline film. We showed that this can be realized by using a mildly humid environment (1.0% H_2O in air) which promotes lattice shrinkage in a rapid way while avoiding significant grain boundary defects introduced by the concom-

https://doi.org/10.1021/acs.chemmater.1c00455
Chem. Mater. 2021, 33, 4035–4044

itant shrinkage in grain size. For example, heat treatment in the dry environment does not lead to a significant change in the lattice parameter (0.2%) even when the treatment temperature was much higher, and to achieve a 0.2% shrinkage in lattice parameter under a dry environment, it will inevitably induce a large shrinkage in the grain size which would lead to severe crack formation for polycrystalline ZIF-8 films.

The stiffened ZIF-8 will improve the feasibility of high-performance carbon capture membranes either from polycrystalline films or from mixed-matrix membranes. This finding can evolve into a generic method for addressing the flexibility of a large number of MOFs. The method is expected to be replicable for the ZIF family including several ZIFs for gas separations (ZIF-7, ZIF-67, ZIF-90, etc.) for obtaining a tight molecular cutoff from their membranes.

4. EXPERIMENTAL SECTION

Synthesis and the Heat Treatment of ZIF-8 Membranes. ZIF-8 membranes were synthesized on an anodic aluminum oxide (AAO) substrate (pore opening: 100 nm; diameter: 13 mm; Whatman, General Electric) by the previously reported electrophoretic nuclei assembly for crystallization of highly intergrown thin-films (ENACT) method.[22,23] After depositing an ∼100 nm thick layer of ZIF-8 nuclei, an ∼800 nm thick film was grown by secondary growth for 60 min followed by repeating the growth in fresh growth precursor solution for 60 min (Figure 1a). The heat treatment of ZIF-8 membranes was conducted in the rapid heat treatment (RHT) setup as described in our previous work[27] (Figure S1). Briefly, ZIF-8 membranes were loaded in a homemade stainless steel sample holder and placed in the center of a quartz tube inside a tubular furnace. Both ends of the tubes were open to the ambient air. The humidity of the atmosphere in the furnace was altered by flowing humidified air through one side of the tube. After a certain heat treatment dwell time, ZIF-8 membranes were taken out of the furnace immediately.

Synthesis of ZIF-8 Crystal. For *in situ* XRD measurements, ZIF-8 was crystallized for 10 h from the precursor solution during the membrane synthesis. The crystals were centrifuged, washed by methanol, and dried before use. The larger ZIF-8 crystal, with size in the range 10−25 μm, was synthesized by a formate-modulated solvothermal approach reported by Cravillon et al.[43] Briefly, first, 0.532 g of zinc chloride ($ZnCl_2$, Sigma-Aldrich, ≥97%) and 0.487 g of 2-methylimidazole (Hmim, Acros Organics, 99%) were dissolved separately in 40 mL of methanol. After another 0.272 g of sodium formate ($NaHCO_2$, TCI, >97.0%) was dissolved in Hmim solution, the two solutions were mixed and added into a solvothermal reactor. The crystallization was performed at 130 °C for 4 h. The resulting ZIF-8 crystals were centrifuged, washed by methanol, and dried before use.

Heat Treatment of ZIF-8 Crystal. For observation of the size change, a small amount of ZIF-8 crystals was dispersed in 20 mL of ethanol. Then, a few drops of ZIF-8 dispersion were added on a premarked silicon wafer (1.5 × 1.5 cm^2). SEM images of ZIF-8 crystals in the vicinity of the markers on the silicon wafer were collected before heat treatment. For other characterizations, the vacuum-dried ZIF-8 powder was used. The heat treatment of ZIF-8 was conducted in a three-zone tube furnace (Nabertherm) under argon, ambient air, and water vapor atmospheres. For heating in argon, the furnace was swept with argon at a flow rate of 0.4 L min^{-1}. For heating in ambient air, the tube was open to ambient atmosphere. For heating in humid environments, the tube was swept with water vapor produced by bubbling compressed air into a 70 °C water bath as described in Note S1. After the heat treatment, SEM images of the marked ZIF-8 crystals on the silicon wafer were collected to compare the size change before and after heating.

■ ASSOCIATED CONTENT

Supporting Information

The Supporting Information is available free of charge at https://pubs.acs.org/doi/10.1021/acs.chemmater.1c00455.

Notes; characterization methods; supplementary SEM images, and other characterization data; schematic of the experimental setups, and detailed gas permeation data of membranes (PDF)

■ AUTHOR INFORMATION

Corresponding Author

Kumar Varoon Agrawal − *Laboratory of Advanced Separations (LAS), École Polytechnique Fédérale de Lausanne (EPFL), CH-1951 Sion, Switzerland;* orcid.org/0000-0002-5170-6412; Email: kumar.agrawal@epfl.ch

Authors

Jian Hao − *Laboratory of Advanced Separations (LAS), École Polytechnique Fédérale de Lausanne (EPFL), CH-1951 Sion, Switzerland;* orcid.org/0000-0002-2838-7652

Deepu J. Babu − *Laboratory of Advanced Separations (LAS), École Polytechnique Fédérale de Lausanne (EPFL), CH-1951 Sion, Switzerland*

Qi Liu − *Laboratory of Advanced Separations (LAS), École Polytechnique Fédérale de Lausanne (EPFL), CH-1951 Sion, Switzerland;* orcid.org/0000-0002-9377-8529

Pascal Alexander Schouwink − *Institut des Sciences et Ingénierie Chimiques, EPFL, CH-1951 Sion, Switzerland*

Mehrdad Asgari − *Laboratory for Functional Inorganic Materials (LFIM), EPFL, CH-1951 Sion, Switzerland*

Wendy L. Queen − *Laboratory for Functional Inorganic Materials (LFIM), EPFL, CH-1951 Sion, Switzerland;* orcid.org/0000-0002-8375-2341

Complete contact information is available at: https://pubs.acs.org/10.1021/acs.chemmater.1c00455

Notes

The authors declare no competing financial interest.

■ ACKNOWLEDGMENTS

The authors acknowledge the home institution, EPFL, for generous support. A part of the project was funded by the Swiss National Science Foundation (SNSF) Assistant Professor Energy Grant (PYAPP2_173645) and European Research Council (ERC) starting grant (805437 Ultimate Membranes).

■ REFERENCES

(1) Park, K. S.; Ni, Z.; Cote, A. P.; Choi, J. Y.; Huang, R.; Uribe-Romo, F. J.; Chae, H. K.; O'Keeffe, M.; Yaghi, O. M. Exceptional Chemical and Thermal Stability of Zeolitic Imidazolate Frameworks. *Proc. Natl. Acad. Sci. U. S. A.* **2006**, *103* (27), 10186−10191.

(2) Banerjee, R.; Phan, A.; Wang, B.; Knobler, C.; Furukawa, H.; O'Keeffe, M.; Yaghi, O. M. High-Throughput Synthesis of Zeolitic Imidazolate Frameworks and Application to CO_2 Capture. *Science* **2008**, *319* (5865), 939−943.

(3) Li, K.; Olson, D. H.; Seidel, J.; Emge, T. J.; Gong, H.; Zeng, H.; Li, J. Zeolitic Imidazolate Frameworks for Kinetic Separation of Propane and Propene. *J. Am. Chem. Soc.* **2009**, *131* (30), 10368−10369.

(4) McCarthy, M. C.; Varela-Guerrero, V.; Barnett, G. V.; Jeong, H. K. Synthesis of Zeolitic Imidazolate Framework Films and Membranes with Controlled Microstructures. *Langmuir* **2010**, *26* (18), 14636−14641.

(5) Bux, H.; Feldhoff, A.; Cravillon, J.; Wiebcke, M.; Li, Y. S.; Caro, J. Oriented Zeolitic Imidazolate Framework-8 Membrane with Sharp H 2/C3H8Molecular Sieve Separation. *Chem. Mater.* **2011**, *23* (8), 2262−2269.
(6) Zhang, C.; Lively, R. P.; Zhang, K.; Johnson, J. R.; Karvan, O.; Koros, W. J. Unexpected Molecular Sieving Properties of Zeolitic Imidazolate Framework-8. *J. Phys. Chem. Lett.* **2012**, *3* (16), 2130−2134.
(7) Bachman, J. E.; Smith, Z. P.; Li, T.; Xu, T.; Long, J. R. Enhanced Ethylene Separation and Plasticization Resistance in Polymer Membranes Incorporating Metal-Organic Framework Nanocrystals. *Nat. Mater.* **2016**, *15* (8), 845−849.
(8) Ma, X.; Kumar, P.; Mittal, N.; Khlyustova, A.; Daoutidis, P.; Mkhoyan, K. A.; Tsapatsis, M. Zeolitic Imidazolate Framework Membranes Made by Ligand-Induced Permselectivation. *Science* **2018**, *361* (6406), 1008−1011.
(9) Zhao, D.; Timmons, D. J.; Yuan, D.; Zhou, H. C. Tuning the Topology and Functionality of Metal-Organic Frameworks by Ligand Design. *Acc. Chem. Res.* **2011**, *44* (2), 123−133.
(10) Thompson, J. A.; Blad, C. R.; Brunelli, N. A.; Lydon, M. E.; Lively, R. P.; Jones, C. W.; Nair, S. Hybrid Zeolitic Imidazolate Frameworks: Controlling Framework Porosity and Functionality by Mixed-Linker Synthesis. *Chem. Mater.* **2012**, *24* (10), 1930−1936.
(11) Jayachandrababu, K. C.; Sholl, D. S.; Nair, S. Structural and Mechanistic Differences in Mixed-Linker Zeolitic Imidazolate Framework Synthesis by Solvent Assisted Linker Exchange and de Novo Routes. *J. Am. Chem. Soc.* **2017**, *139* (16), 5906−5915.
(12) Eum, K.; Hayashi, M.; De Mello, M. D.; Xue, F.; Kwon, H. T.; Tsapatsis, M. ZIF-8 Membrane Separation Performance Tuning by Vapor Phase Ligand Treatment. *Angew. Chem., Int. Ed.* **2019**, *58* (46), 1−5.
(13) Knebel, A.; Geppert, B.; Volgmann, K.; Kolokolov, D. I.; Stepanov, A. G.; Twiefel, J.; Heitjans, P.; Volkmer, D.; Caro, J. Defibrillation of Soft Porous Metal-Organic Frameworks with Electric Fields. *Science* **2017**, *358* (6361), 347−351.
(14) Li, L.; Zhang, L.; Duan, Y.; Caro, J.; Wang, H.; Hou, Q.; Zhou, S.; Wei, Y.; Ding, L.-X.; Xue, J. Paralyzed Membrane: Current-Driven Synthesis of a Metal-Organic Framework with Sharpened Propene/Propane Separation. *Sci. Adv.* **2018**, *4* (10), eaau1393.
(15) Polyukhov, D. M.; Poryvaev, A. S.; Gromilov, S. A.; Fedin, M. V. Precise Measurement and Controlled Tuning of Effective Window Sizes in ZIF-8 Framework for Efficient Separation of Xylenes. *Nano Lett.* **2019**, *19* (9), 6506−6510.
(16) Hou, Q.; Wu, Y.; Zhou, S.; Wei, Y.; Caro, J.; Wang, H. Ultra-Tuning of the Aperture Size in Stiffened ZIF-8_Cm Frameworks with Mixed-Linker Strategy for Enhanced CO_2/CH4 Separation. *Angew. Chem., Int. Ed.* **2019**, *58* (1), 327−331.
(17) Sun, J.; Semenchenko, L.; Lim, W. T.; Ballesteros Rivas, M. F.; Varela-Guerrero, V.; Jeong, H. K. Facile Synthesis of Cd-Substituted Zeolitic-Imidazolate Framework Cd-ZIF-8 and Mixed-Metal CdZn-ZIF-8. *Microporous Mesoporous Mater.* **2018**, *264*, 35−42.
(18) Hao, J.; Babu, D. J.; Liu, Q.; Chi, H.-Y.; Lu, C.; Liu, Y.; Agrawal, K. V. Synthesis of High-Performance Polycrystalline Metal−Organic Framework Membranes at Room Temperature in a Few Minutes. *J. Mater. Chem. A* **2020**, *8* (16), 7633−7640.
(19) Shekhah, O.; Eddaoudi, M. The Liquid Phase Epitaxy Method for the Construction of Oriented ZIF-8 Thin Films with Controlled Growth on Functionalized Surfaces. *Chem. Commun.* **2013**, *49* (86), 10079−10081.
(20) Li, W.; Su, P.; Li, Z.; Xu, Z.; Wang, F.; Ou, H.; Zhang, J.; Zhang, G.; Zeng, E. Ultrathin Metal-Organic Framework Membrane Production by Gel-Vapour Deposition. *Nat. Commun.* **2017**, *8* (1), 1−8.
(21) Kwon, H. T.; Jeong, H. K. Highly Propylene-Selective Supported Zeolite-Imidazolate Framework (ZIF-8) Membranes Synthesized by Rapid Microwave-Assisted Seeding and Secondary Growth. *Chem. Commun.* **2013**, *49* (37), 3854−3856.
(22) He, G.; Dakhchoune, M.; Zhao, J.; Huang, S.; Agrawal, K. V. Electrophoretic Nuclei Assembly for Crystallization of High-Performance Membranes on Unmodified Supports. *Adv. Funct. Mater.* **2018**, *28* (20), 1707427.
(23) He, G.; Babu, D. J.; Agrawal, K. V. Electrophoretic Crystallization of Ultrathin High-Performance Metal-Organic Framework Membranes. *J. Visualized Exp.* **2018**, No. 138, e58301.
(24) Fairen-Jimenez, D.; Moggach, S. A.; Wharmby, M. T.; Wright, P. A.; Parsons, S.; Düren, T. Opening the Gate: Framework Flexibility in ZIF-8 Explored by Experiments and Simulations. *J. Am. Chem. Soc.* **2011**, *133* (23), 8900−8902.
(25) Moggach, S. A.; Bennett, T. D.; Cheetham, A. K. The Effect of Pressure on ZIF-8: Increasing Pore Size with Pressure and the Formation of a High-Pressure Phase at 1.47 GPa. *Angew. Chem., Int. Ed.* **2009**, *48* (38), 7087−7089.
(26) Pan, Y.; Li, T.; Lestari, G.; Lai, Z. Effective Separation of Propylene/Propane Binary Mixtures by ZIF-8 Membranes. *J. Membr. Sci.* **2012**, *390*−*391*, 93−98.
(27) Babu, D. J.; He, G.; Hao, J.; Vahdat, M. T.; Schouwink, P. A.; Mensi, M.; Agrawal, K. V. Restricting Lattice Flexibility in Polycrystalline Metal-Organic Framework Membranes for Carbon Capture. *Adv. Mater.* **2019**, *31* (28), 1900855.
(28) Zhang, C.; Koros, W. J. Tailoring the Transport Properties of Zeolitic Imidazolate Frameworks by Post-Synthetic Thermal Modification. *ACS Appl. Mater. Interfaces* **2015**, *7* (42), 23407−23411.
(29) Gadipelli, S.; Travis, W.; Zhou, W.; Guo, Z. A Thermally Derived and Optimized Structure from ZIF-8 with Giant Enhancement in CO_2 Uptake. *Energy Environ. Sci.* **2014**, *7* (7), 2232−2238.
(30) James, J. B.; Lin, Y. S. Kinetics of ZIF-8 Thermal Decomposition in Inert, Oxidizing, and Reducing Environments. *J. Phys. Chem. C* **2016**, *120* (26), 14015−14026.
(31) James, J. B.; Lin, Y. S. Thermal Stability of ZIF-8 Membranes for Gas Separations. *J. Membr. Sci.* **2017**, *532*, 9−19.
(32) Zhang, H.; Liu, D.; Yao, Y.; Zhang, B.; Lin, Y. S. Stability of ZIF-8 Membranes and Crystalline Powders in Water at Room Temperature. *J. Membr. Sci.* **2015**, *485*, 103−111.
(33) Jiang, H. L.; Liu, B.; Lan, Y. Q.; Kuratani, K.; Akita, T.; Shioyama, H.; Zong, F.; Xu, Q. From Metal-Organic Framework to Nanoporous Carbon: Toward a Very High Surface Area and Hydrogen Uptake. *J. Am. Chem. Soc.* **2011**, *133* (31), 11854−11857.
(34) Chaikittisilp, W.; Hu, M.; Wang, H.; Huang, H.-S.; Fujita, T.; Wu, K. C. W.; Chen, L.-C.; Yamauchi, Y.; Ariga, K. Nanoporous Carbons through Direct Carbonization of a Zeolitic Imidazolate Framework for Supercapacitor Electrodes. *Chem. Commun.* **2012**, *48* (58), 7259.
(35) Torad, N. L.; Hu, M.; Kamachi, Y.; Takai, K.; Imura, M.; Naito, M.; Yamauchi, Y. Facile Synthesis of Nanoporous Carbons with Controlled Particle Sizes by Direct Carbonization of Monodispersed ZIF-8 Crystals. *Chem. Commun.* **2013**, *49* (25), 2521−2523.
(36) Sun, J. K.; Xu, Q. Functional Materials Derived from Open Framework Templates/Precursors: Synthesis and Applications. *Energy Environ. Sci.* **2014**, *7* (7), 2071−2100.
(37) Yin, H.; Kim, H.; Choi, J.; Yip, A. C. K. Thermal Stability of ZIF-8 under Oxidative and Inert Environments: A Practical Perspective on Using ZIF-8 as a Catalyst Support. *Chem. Eng. J.* **2015**, *278*, 293−300.
(38) Pan, T.; Shen, Y.; Wu, P.; Gu, Z.; Zheng, B.; Wu, J.; Li, S.; Fu, Y.; Zhang, W.; Huo, F. Thermal Shrinkage Behavior of Metal−Organic Frameworks. *Adv. Funct. Mater.* **2020**, *30* (34), 2001389.
(39) Bux, H.; Liang, F.; Li, Y.; Cravillon, J.; Wiebcke, M.; Caro, J. Zeolitic Imidazolate Framework Membrane with Molecular Sieving Properties by Microwave-Assisted Solvothermal Synthesis. *J. Am. Chem. Soc.* **2009**, *131* (44), 16000−16001.
(40) Pinnau, I.; Casillas, C. G.; Morisato, A.; Freeman, B. D. Hydrocarbon/Hydrogen Mixed Gas Permeation in Poly(1-Trimethylsilyl-1-Propyne) (PTMSP), Poly(1-Phenyl-1-Propyne) (PPP), and PTMSP/PPP Blends. *J. Polym. Sci., Part B: Polym. Phys.* **1996**, *34* (15), 2613−2621.
(41) Bouëssel Du Bourg, L.; Ortiz, A. U.; Boutin, A.; Coudert, F. X. Thermal and Mechanical Stability of Zeolitic Imidazolate Frameworks Polymorphs. *APL Mater.* **2014**, *2* (12), 124110.

https://doi.org/10.1021/acs.chemmater.1c00455
Chem. Mater. 2021, 33, 4035−4044

(42) Cravillon, J.; Schröder, C. A.; Bux, H.; Rothkirch, A.; Caro, J.; Wiebcke, M. Formate Modulated Solvothermal Synthesis of ZIF-8 Investigated Using Time-Resolved in Situ X-Ray Diffraction and Scanning Electron Microscopy. *CrystEngComm* **2012**, *14* (2), 492−498.
(43) Cravillon, J.; Münzer, S.; Lohmeier, S.-J.; Feldhoff, A.; Huber, K.; Wiebcke, M. Rapid Room-Temperature Synthesis and Characterization of Nanocrystals of a Prototypical Zeolitic Imidazolate Framework. *Chem. Mater.* **2009**, *21* (8), 1410−1412.
(44) Avci, C.; Ariñez-Soriano, J.; Carné-Sánchez, A.; Guillerm, V.; Carbonell, C.; Imaz, I.; Maspoch, D. Post-Synthetic Anisotropic Wet-Chemical Etching of Colloidal Sodalite ZIF Crystals. *Angew. Chem., Int. Ed.* **2015**, *54* (48), 14417−14421.
(45) Zhang, C.; Han, C.; Sholl, D. S.; Schmidt, J. R. Computational Characterization of Defects in Metal−Organic Frameworks: Spontaneous and Water-Induced Point Defects in ZIF-8. *J. Phys. Chem. Lett.* **2016**, *7* (3), 459−464.
(46) Liu, X.; Li, Y.; Ban, Y.; Peng, Y.; Jin, H.; Bux, H.; Xu, L.; Caro, J.; Yang, W. Improvement of Hydrothermal Stability of Zeolitic Imidazolate Frameworks. *Chem. Commun.* **2013**, *49* (80), 9140−9142.
(47) Öztürk, Z.; Filez, M.; Weckhuysen, B. M. Decoding Nucleation and Growth of Zeolitic Imidazolate Framework Thin Films with Atomic Force Microscopy and Vibrational Spectroscopy. *Chem. - Eur. J.* **2017**, *23* (45), 10915−10924.
(48) Hu, Y.; Kazemian, H.; Rohani, S.; Huang, Y.; Song, Y. In Situ High Pressure Study of ZIF-8 by FTIR Spectroscopy. *Chem. Commun.* **2011**, *47* (47), 12694−12696.
(49) Hadjiivanov, K. I.; Vayssilov, G. N. Characterization of Oxide Surfaces and Zeolites by Carbon Monoxide as an IR Probe Molecule. *Adv. Catal.* **2002**, *47*, 307−511.
(50) Bloch, E. D.; Hudson, M. R.; Mason, J. A.; Chavan, S.; Crocellà, V.; Howe, J. D.; Lee, K.; Dzubak, A. L.; Queen, W. L.; Zadrozny, J. M.; Geier, S. J.; Lin, L. C.; Gagliardi, L.; Smit, B.; Neaton, J. B.; Bordiga, S.; Brown, C. M.; Long, J. R. Reversible CO Binding Enables Tunable CO/H2 and CO/N2 Separations in Metal-Organic Frameworks with Exposed Divalent Metal Cations. *J. Am. Chem. Soc.* **2014**, *136* (30), 10752−10761.

https://doi.org/10.1021/acs.chemmater.1c00455
Chem. Mater. 2021, 33, 4035−4044